

General Disclaimer

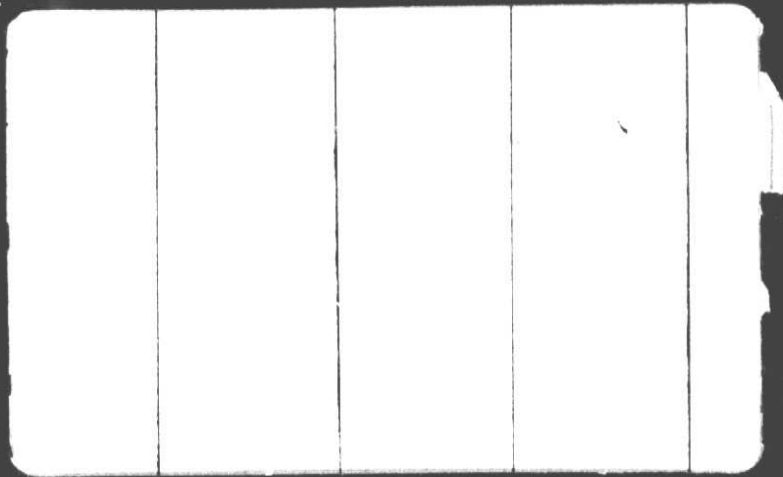
One or more of the Following Statements may affect this Document

- This document has been reproduced from the best copy furnished by the organizational source. It is being released in the interest of making available as much information as possible.
- This document may contain data, which exceeds the sheet parameters. It was furnished in this condition by the organizational source and is the best copy available.
- This document may contain tone-on-tone or color graphs, charts and/or pictures, which have been reproduced in black and white.
- This document is paginated as submitted by the original source.
- Portions of this document are not fully legible due to the historical nature of some of the material. However, it is the best reproduction available from the original submission.

MASSACHUSETTS INSTITUTE OF TECHNOLOGY

Department of Ocean Engineering

Cambridge, Massachusetts 02139



(NASA-CR-144074) ANALYSIS OF THERMAL
STRESSES AND METAL MOVEMENT DURING WELDING
Final Report (Massachusetts Inst. of Tech.)
43 p HC \$4.00 CSCI 13H

G3/37

Unclas
05093

N76-13497



MASSACHUSETTS INSTITUTE OF TECHNOLOGY
DEPARTMENT OF OCEAN ENGINEERING
CAMBRIDGE, MASS. 02139

Final Report

Under Contract No. NAS8-24365

M.I.T. DSR 71648

Analysis of Thermal Stresses and
Metal Movement During Welding

by

T. Muraki
F. M. Pattee
and
K. Masubuchi

to

George C. Marshall Space Flight Center
National Aeronautics and Space Administration

June 30, 1974

Report No. 74-12

TABLE OF CONTENTS

Summary.....	ii
1.0 Introduction and Scope of the Extended Research Contract.....	1
2.0 Theoretical Analysis of Thermal Stresses and Metal Movement During Welding.....	2
2.1 Introduction and Background.....	2
2.2 Mathematical Formulation of Thermal Elasto- Plastic Problems.....	4
2.3 Stress Conditions in Regions Near the Heat Source.....	9
2.4 Analysis of Heat Flow.....	10
2.5 Material Properties.....	12
3.0 Phase G: Experiments on Thermal Stresses and Metal Movement During Bead-On-Plate Weld Along the Girth of a Cylindrical Shell.....	15
3.1 Introduction.....	15
3.2 Apparatus and Procedure.....	15
3.3 Experimental Operation.....	24
3.4 Experimental Results and Analyses.....	26
References.....	37

SUMMARY

This is the final report of Contract No. NAS8-24365. This report covers the following tasks, conducted during the period from July 1, 1973 through June 30, 1974:

- (1) Complete description of theoretical studies
- (2) Phase G: Perform experiments on thermal stresses and metal movement in joining thin cylindrical shells.

Results of the earlier work are described in the following two reports:

- a. NASA Contracts Report CR-61351, which covers the work performed during the period from May 15, 1969 to October 14, 1970.
- b. Phase Report, which covers the work performed during the period from October 15, 1970 to June 30, 1973.

The first part of this final report describes the theoretical analysis of thermal stresses and metal movement during welding. Finite-element computer programs have been developed to determine thermal stresses and metal movement during butt welding of flat plates and bead-on-plate welding along the girth of a cylindrical shell.

The second part of the report describes results of experiments on circular cylindrical shells in 6061 aluminum alloy. Measurements were made on changes of temperature and thermal strains during bead-on-plate welding (by gas tungsten-arc process) along the girth of the cylindrical shell.

1.0 INTRODUCTION AND SCOPE OF THE EXTENDED
RESEARCH CONTRACT

The original research contract on "Analysis of Thermal Stresses and Metal Movement during Welding" was initiated on May 15, 1969 with an appropriation of \$35,390. The study was completed on October 14, 1970, and the final report of the study was published on December 15, 1970, as the NASA Contractor Report CR-61351. (1)

The extension of the contract became effective on October 14, 1970 with an appropriation of \$19,735. In June 1972, the contract was further extended with an additional appropriation of \$10,000. A phase report was prepared to cover the work from October 15, 1970 to June 30, 1973. (2) This report covers primarily the work from July 1, 1973 through June 30, 1974.

As described in the phase report, the study from July 1, 1973 through June 30, 1974 covers:

- (1) Complete description of theoretical studies
- (2) Phase G: Perform experiments on thermal stresses and metal movement in joining thin cylindrical shells.

2.0 THEORETICAL ANALYSIS OF THERMAL STRESSES AND METAL MOVEMENT DURING WELDING

2.1 Introduction and Background

One of the troublesome problems that accompanies the construction of welded structures is residual stresses and distortion. Because a weldment is locally heated, the temperature distribution is not uniform and changes during welding. This nonuniform temperature distribution causes thermal stresses and resulting residual stresses.

A number of research programs have been carried out on residual stresses and distortion in weldments. Several reviews and books have been written on various subjects related to residual stresses and distortion in weldments. (3,4)

Until recently, however, almost all studies were on residual stresses and distortion after welding is completed and only limited studies were made on transient thermal stresses and metal movement.* This is due to the complexity of the problem characterized by large temperature changes in small areas near the welding arc with its resulting non-elastic deformation, temperature dependency of the material properties and/or phase transformations, and complex boundary conditions resulting from conditions of geometry and multi-pass welding.

With the advancement of the computer technology, it is now possible to analyze, with reasonable cost and time, thermal stresses and metal movement. Investigators at M.I.T. and some other lab-

* WRC 149 (3) discusses the present state-of-the-art of analysis of residual stresses and distortion of weldments.

3

oratories in the world are currently developing computer programs on thermal stresses during welding and other related subjects.*

For example, finite-element programs on welding thermal stresses have been developed by Hibbit and Marcel⁽⁵⁾, Ueda and Yamakawa^(6,7), and Nomoto⁽⁸⁾.

At M.I.T., a systematic research has been conducted since 1968 on heat flow during welding, transient thermal stresses, residual stresses and distortion. The research includes analytical and experimental studies.

The analysis was started with the development of a simple one-dimensional program on a bead-on-plate weld.^(9,1) The analysis has been expanded to a two-dimensional program which can analyze stresses during welding a butt joint. Efforts have been made to analyze thermal stresses during welding a cylindrical shell.

In the analytical study, elasto-plastic finite-element computer programs have been developed on thermal stresses and metal movement during welding. A finite-element formulation has been derived in the general form which includes temperature dependence of material properties and the yield criterion.

* To coordinate these efforts, Commission X (Residual Stress, Stress Relieving, and Brittle Fracture) of the International Institute of Welding established in 1972 a working group on "Numerical Analyses of Stresses, Strains, and Other Effects Produced by Welding." Professor K. Masubuchi, of M.I.T. is the chairman of the working group. The working group plans to prepare within a year or two a report covering studies being made in various laboratories in the world.

2.2 Mathematical Formulation of Thermal Elasto-Plastic Problems

Constitutive Equations. One of the important features in the analysis of thermal stresses and distortion during welding is the temperature dependency of material properties and the yield criterion. (4,10,11,12)

Therefore, general constitutive equations are provided for the analysis of thermal stresses. The rate of strain is, in general,

$$\dot{\epsilon}_{ij} = \dot{\epsilon}_{ij}^{(e)} + \dot{\epsilon}_{ij}^{(p)} \quad (1)$$

where superscripts, e and p refer to elastic and plastic strains, respectively.

The rate of plastic strain is assumed as

$$\dot{\epsilon}_{ij}^{(p)} = \Lambda \frac{\partial f}{\partial \sigma_{ij}} \quad (2)$$

where Λ , f , and σ_{ij} are the proportional constant, the yield function, and the stress component, respectively.

The yield function is assumed as

$$f(\sigma_{ij}^{(p)}, \epsilon_{ij}^{(p)}, \kappa(\epsilon_{ij}^{(p)}), T) = 0 \quad (3)$$

where κ is the parameter related to the strain hardening of material and T is temperature.

Differentiating Eq. (3) and using the result with Eq. (2), the following relationship is obtained.

$$\dot{\epsilon}_{ij}^{(p)} = \hat{G} \left(\frac{\partial f}{\partial \sigma_{ij}} \frac{\partial f}{\partial \sigma_{kl}} \dot{\sigma}_{kl} + \frac{\partial f}{\partial \sigma_{ij}} \frac{\partial f}{\partial T} \dot{T} \right) \quad (4)$$

where

$$\hat{G} = - \frac{1}{\left(\frac{\partial f}{\partial \epsilon_{ij}^{(p)}} + \frac{\partial f}{\partial \kappa} \frac{\partial \kappa}{\partial \epsilon_{ij}^{(p)}} \right) \frac{\partial f}{\partial \sigma_{ij}}} \quad (5)$$

If von Mises' yield criterion is adopted, the temperature dependency can be considered in it as,

$$f = \bar{\sigma} - c(\epsilon_{ij}^{(p)}, T) \quad (6)$$

where c is the parameter related to the strain hardening of the material and $\bar{\sigma}$ is defined in the form as

$$\bar{\sigma} = \sqrt{\frac{3}{2}} \sqrt{\sigma'_{ij} \sigma'_{ij}} \quad (7)$$

where σ'_{ij} is the stress deviation.

Using Eq. (6), Eq. (5) becomes

$$\hat{G} = - \frac{1}{\frac{\partial f}{\partial \epsilon_{ij}^{(p)}} \frac{\partial f}{\partial \sigma_{ij}}} \quad (8)$$

.. Here, introducing the rate of equivalent strain,

$$\dot{\bar{\epsilon}}^{(p)} = \sqrt{\frac{2}{3}} \sqrt{\dot{\epsilon}_{ij}^{(p)} \dot{\epsilon}_{ij}^{(p)}} \quad (9)$$

and then, using Eqs. (2) and (6), we have

$$1 = \frac{\partial f}{\partial \sigma_{ij}} \frac{\partial \bar{\epsilon}^{(p)}}{\partial \epsilon_{ij}^{(p)}} \quad (10)$$

Hence, Eq. (8) becomes

$$\hat{G} = - \frac{1}{\frac{\partial f}{\partial \epsilon_{ij}^{(p)}} \cdot \frac{\partial \epsilon_{ij}^{(p)}}{\partial \bar{\epsilon}^{(p)}}} = \frac{1}{H'} \quad (11)$$

where

$$H' = - \frac{\partial f}{\partial \bar{\epsilon}^{(p)}} \quad (12)$$

Finally, using Eqs. (6), (7), and (11), the rate of plastic strain becomes

$$\dot{\epsilon}_{ij}^{(p)} = \frac{1}{H'} \left(\frac{3\sigma'_{ij}}{2\bar{\sigma}} \frac{3\sigma'_{kl}}{2\bar{\sigma}} \dot{\sigma}_{kl} + \frac{3\sigma'_{ij}}{2\bar{\sigma}} \frac{\partial f}{\partial T} \dot{T} \right) \quad (13.1)$$

or:

$$\dot{\epsilon}_{ij}^{(p)} = \frac{1}{H'} \left(\frac{3\sigma'_{ij}}{2\bar{\sigma}} \dot{\bar{\sigma}} + \frac{3\sigma'_{ij}}{2\bar{\sigma}} \frac{\partial f}{\partial T} \dot{T} \right) \quad (13.2)$$

Equation (13) means that if the temperature dependency of the yield function is taken into account in the form as Eq. (6), the effect of temperature is given as the additional term to the well-known relation between strain and stress rates. From the above derivation, it is also obvious that the more general relation is obtained if necessary.

For the elastic part, we have:

$$\dot{\epsilon}_{ij}^{(e)} = \frac{1-2\nu}{E} \dot{\sigma} \delta_{ij} + \frac{\dot{\sigma}'_{ij}}{2G} - \frac{1-2\nu}{E^2} E \dot{\sigma} \delta_{ij} - \frac{1}{2G^2} G \dot{\sigma}'_{ij} + \dot{\epsilon}^{\theta} \delta_{ij} \quad (14)$$

where, σ and δ_{ij} are the average hydrostatic stress and Kronecker symbol, respectively. ν , and G are Poisson's ratio, Young's Modulus and shear modulus, respectively. ϵ^{θ} denotes the thermal strain caused by the temperature distribution.

Substituting Eqs. (13) and (14) into Eq. (1), the total strain rate becomes

$$\begin{aligned} \dot{\epsilon}_{ij} = & \frac{1-2\nu}{E} \dot{\sigma}_{ij} + \frac{\ddot{\sigma}_{ij}}{2G} + \frac{3\sigma'_{ij}}{2\bar{\sigma}H'} \dot{\bar{\sigma}} + \dot{\epsilon}^{\theta}_{ij} \\ & - \frac{1-2\nu}{E^2} \dot{E}\sigma_{ij} - \frac{1}{2G^2} \dot{G}\sigma'_{ij} + \frac{3\sigma'_{ij}}{2\bar{\sigma}H'} \frac{\partial f}{\partial T} \dot{T} \end{aligned} \quad (15)$$

The inverse relation of Eq. (15) becomes:

$$\dot{\sigma}_{ij} = \frac{E}{1-2\nu} \dot{\epsilon}_{ij} + 2G\dot{\epsilon}'_{ij} - \frac{3G\sigma'_{ij}\sigma'_{kl}\dot{\epsilon}_{kl}}{\bar{\sigma}^2\left(\frac{H'}{3G} + 1\right)} + \dot{\sigma}^{\theta}_{ij} \quad (16)$$

where,

$$\epsilon = \frac{1}{3} \epsilon_{ii}$$

$$\begin{aligned} \dot{\sigma}^{\theta}_{ij} = & - \frac{E}{1-2\nu} \dot{\epsilon}^{\theta}_{ij} + \frac{\sigma}{E} \dot{E}\delta_{ij} + \frac{\sigma'_{ij}}{G} \left\{ 1 - \frac{1}{\left(\frac{H'}{3G} + 1\right)} \right\} \dot{G} \\ & - \frac{3G\sigma'_{ij}}{\bar{\sigma}H'} \frac{\partial f}{\partial T} \left\{ 1 - \frac{1}{\left(\frac{H'}{3G} + 1\right)} \right\} \dot{T} \end{aligned} \quad (17)$$

$\dot{\sigma}^{\theta}_{ij}$ consists of the terms related to the rate of thermal strain and the temperature dependency of the material properties and the yield criterion.

If an element in question is plastic, the element takes one of the following states at the next time increment:

$$\begin{aligned} f = 0 \quad \dot{f}' < 0 & \quad (\text{unloading}) \\ f = 0 \quad \dot{f}' = 0 & \quad (\text{neutral}) \\ f = 0 \quad \dot{f}' > 0 & \quad (\text{loading}) \end{aligned} \quad (18)$$

$$\text{where } \dot{f}' = \frac{\partial f}{\partial \sigma_{ij}} \dot{\sigma}_{ij} + \frac{\partial f}{\partial T} \dot{T}.$$

If the yield function does not move and does not change the size, the loading in the element does not occur. In other words, the unloading or neutral state is possible.

The temperature dependency of the material properties and the yield criterion makes the above judgement complex.

Finite-Element Formulation. For the finite-element approach to plate-stretching problems, the principle of virtual work is most convenient, because it is easy to find displacement fields assumed in an element which satisfy the continuity of the fields along interelement boundaries.

$$\iiint_V \dot{\sigma}_{ij} \delta \dot{\epsilon}_{ij} dV - \iiint_V \dot{\bar{P}}_i \delta \dot{u}_i dV - \iint_{S_1} \dot{\bar{F}}_i \delta \dot{u}_i dS = 0 \quad (19)$$

where $\dot{\bar{P}}_i$, $\dot{\bar{F}}_i$, and \dot{u}_i are components of the body force, the surface force and the displacement, respectively. The displacement fields in a basic triangular element are assumed as

$$\begin{aligned} u &= \alpha_0 + \alpha_1 x + \alpha_2 y \\ v &= \alpha_3 + \alpha_4 x + \alpha_5 y \end{aligned} \quad (20)$$

Once the displacement fields are assumed, the derivation of a stiffness matrix and a load vector for an element is arrived at straightforward by using Eqs. (16), (19) and (20).

The final form of Eq. (19) is

$$\begin{aligned} \sum_{i=1}^N \delta \{\dot{q}\}^T [K] \{\dot{q}\} - \sum_{i=1}^N \delta \{\dot{q}\}^T \{\dot{F}_P\} \\ - \sum_{i=1}^N \delta \{\dot{q}\}^T \{\dot{F}_F\} + \sum_{i=1}^N \delta \{\dot{q}\}^T \{\dot{F}_\theta\} = 0 \end{aligned} \quad (21)$$

where

- \dot{q} : nodal displacement vector
- $[K]$: stiffness matrix
- $\{F_p\}$: load vector due to the body forces
- $\{F_f\}$: load vector due to the surface forces
- $\{F_\theta\}$: load vector due to the thermal strain and the effect of temperature dependency on the material properties and the yield criterion
- N : total number of elements
- n_1 : total number of surfaces related to surface forces

Eq. (21) becomes finally,

$$[K] \{\dot{q}\} = \{\dot{F}\} \quad (22)$$

where subscript θ refers to a whole body.

Eq. (22) is valid for each increment of loads which are caused by the increments of body force, surface force and other forces related to the thermal stresses and the effect of temperature dependency of material properties and the yield criterion.

The temperature distribution, uncoupled from the mechanical problem just described, may be approximated by classical finite difference, or finite element techniques. In this paper, analytical solutions for a moving heat source problem on a plate will be used.

2.3 Stress Conditions in Regions Near the Heat Source

An important subject in the analysis of thermal stresses during welding is how to set up conditions of stresses in regions near the welding arc.

In the analysis of thermal stresses during bead-on-plate welding, it was assumed that:

- (1) The molten zone is in the state of zero stress. In other words, stresses are zero in regions where temperatures exceed the melting temperature of the material.
- (2) The solidified material resumes the original material properties. In other words, the weld metal in temperatures below the melting temperature behaves like the original material in the corresponding temperatures.

In the analysis of thermal stresses during butt welding, it was further assumed that:

- (3) The unwelded portion of the joint is in the stress-free condition, except in regions where tack welds are made. Consequently, as the welding arc advances, the stress state in regions near the welding arc changes from the free stress condition before welding to the molten stage and then to the solidified stage.

2.4 Analysis of Heat Flow

Heat flow in a weldment is affected by various factors including thermophysical properties of the material, thermal efficiency of the heat source, heat loss from surfaces of the weldment, initial temperature, and geometry of the weldment.

Much research has been conducted on heat flow during welding.^(13,14) The most significant early work was done by Rosenthal.⁽¹⁵⁾ His study is essentially an analysis of heat conduction in a solid due to a moving heat source (concentrated at a point (three-dimensional)

or along a line (two-dimensional). The well-known equation for the two-dimensional heat flow in the quasi-stationary state due to a line heat source with the intensity q moving at a constant speed, v , along the x -axis of an infinite plate is as follows (see Figure 1):

$$T = T_0 + \frac{q}{2\pi k} e^{-\frac{v}{2\kappa} \xi} K_0\left(\frac{v}{2\kappa} r\right) \quad (23)$$

where,

T : temperature

T_0 : initial temperature

q : intensity of line heat source

k : thermal conductivity

$\kappa = \frac{k}{c\rho}$: thermal diffusivity, where c is specific heat and ρ is density

v : travelling speed of the heat source

$\xi = x-vt$: moving coordinate, where t is time

r : $\sqrt{\xi^2 + y^2}$

$K_0(z)$: the zero order modified Bessel function of the second kind

The intensity of the heat source, q (Joule \cdot m⁻¹ \cdot sec⁻¹) can be expressed as follows:

$$q = \frac{1}{h} \times \eta \times VI \quad (24)$$

h: plate thickness, m.

η : arc efficiency

V: arc voltage, volts

I: welding current, amperes

In this study, the above equations were used in the analysis of heat flow during welding, since they were found to be sufficiently accurate.

Of course, the finite-element method can be used for analyzing heat flow during welding. In a separate study at M.I.T., finite-element computer programs have been developed on heat flow during welding.(16,17). These programs are useful for analyzing heat flow and thermal stresses during welding a joint with a complex geometry.

2.5 Material Properties

One of the problems that we have experienced lack of sufficient data on material properties at elevated temperatures, especially temperatures close to the melting temperatures. However, in the M.I.T. research so far, no attempt has been made to experimentally determine material properties at elevated temperatures. In other words, we have relied upon existing data.

Table 1 lists some properties of Type 6061 aluminum alloy used for the experimental study.

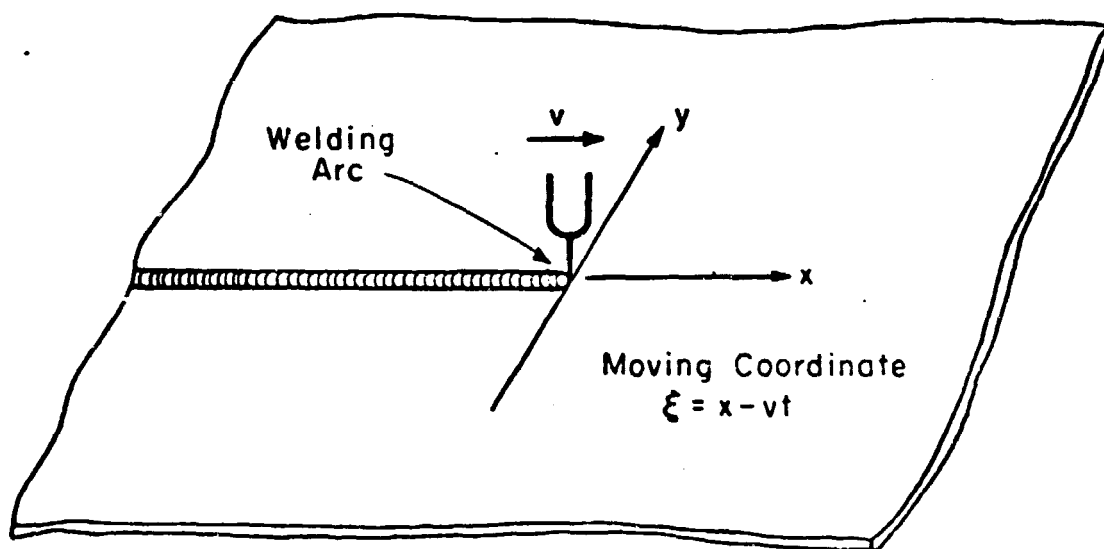


Figure 1 Coordinate System Near the Moving Welding Arc

TEMPERATURE	T	$^{\circ}\text{F}$ ($^{\circ}\text{K}$)	0.0 (255.4)	100.0 (310.9)	200.0 (366.5)	300.0 (422.0)	400.0 (477.6)	500.0 (533.2)	600.0 (588.7)	700.0 (644.3)	800.0 (699.8)	1060.0 (844.3)
Thermal Diffusivity	K	Watt/In ² F (Watt/m ² °K)	2.280 (49.87)	2.389 (52.25)	2.497 (54.62)	2.603 (56.93)	2.712 (59.32)	2.838 (62.07)	2.925 (63.98)	3.062 (66.97)	3.142 (68.72)	3.572 (78.15)
Specific Heat	C	Joule/Lb _m ^{OF} (Joule/kg ^{°K})	227.7 (278.9)	238.2 (291.7)	246.5 (301.9)	253.0 (309.9)	259.0 (317.2)	265.2 (324.8)	271.6 (332.7)	278.1 (340.6)	285.4 (349.6)	310.0 (379.7)
Density	ρ	Lb _m /In ³ (kg/m ³)	0.098 (27.13)	0.097 (26.85)	0.097 (26.85)	0.096 (26.57)	0.096 (26.57)	0.096 (26.57)	0.095 (26.30)	0.095 (26.30)	0.094 (26.02)	0.093 (25.74)
Modulus of Elasticity	E	x 10 ⁻⁶ Psi (MN/m ²)	10.18 (70.19)	9.94 (68.53)	9.60 (66.19)	9.15 (63.09)	8.58 (59.16)	7.83 (53.99)	6.93 (47.78)	5.85 (40.33)	4.60 (31.72)	0.00 (0.00)
Yield Stress	σ _y	Ksi ² (MN/m ²)	40.50 (279.2)	39.80 (274.4)	38.38 (264.6)	36.00 (248.2)	31.70 (218.6)	22.00 (151.7)	9.60 (66.19)	5.00 (34.47)	2.60 (17.93)	0.00 (0.00)
Coefficient of Linear Thermal Expansion	α _T	Microstrain/ [°] F (Microstrain/ [°] K)	12.19 (6.772)	13.03 (7.239)	13.67 (7.594)	14.26 (7.922)	14.78 (8.211)	15.31 (8.506)	15.85 (8.806)	16.43 (9.128)	17.06 (9.478)	19.02 (10.567)
Strain Hardening Parameter	m	-----	0.0742	0.0742	0.0742	0.0742	0.0742	0.0742	0.0742	0.0742	0.0742	0.0742

TABLE 1: SUMMARY OF MECHANICAL AND PHYSICAL PROPERTIES FOR 6061 T6 ALUMINUM ALLOY

3.0 PHASE G: EXPERIMENTS ON THERMAL STRESSES AND METAL MOVEMENT DURING BEAD-ON-PLATE WELD ALONG THE GIRTH OF A CYLINDRICAL SHELL

3.1 Introduction

Three specimens, which were the half of a circular cylindrical shell, were used in the experiments. The specimens were prepared in Type 6061 aluminum alloy. Temperature changes, strain changes and displacements were measured at locations of interest in each experiment. Welding was manually performed by use of gas tungsten-arc (GTA) welding. The first two experiments were considered to be preliminary. From the results obtained by the first two experiments, locations were changed of strain gages and extensimeters. This report covers the third experiment.

3.2 Apparatus and Procedure

Test Specimen: Specimen dimensions and gage locations used are shown in Figure 2. The test specimen is 0.25 inch of thickness, 30 inches in length, and 18 inches in girth. The radius is 5 7/8 inches. The specimen was clamped to a base plate with eight tabs, each four of which were located along longitudinal edges of the shell specimen. A summary of mechanical and physical properties of Type 6061 aluminum alloy used for the specimen is given in Table 1.

Temperature Measurement: All temperature sensors used were Chromel/Alumel thermocouples made from Leads and Northrop No. 28 wires. Each thermocouple was spot-welded onto the test specimen and protected by No. 33 Sauereisen Sealing Cement.

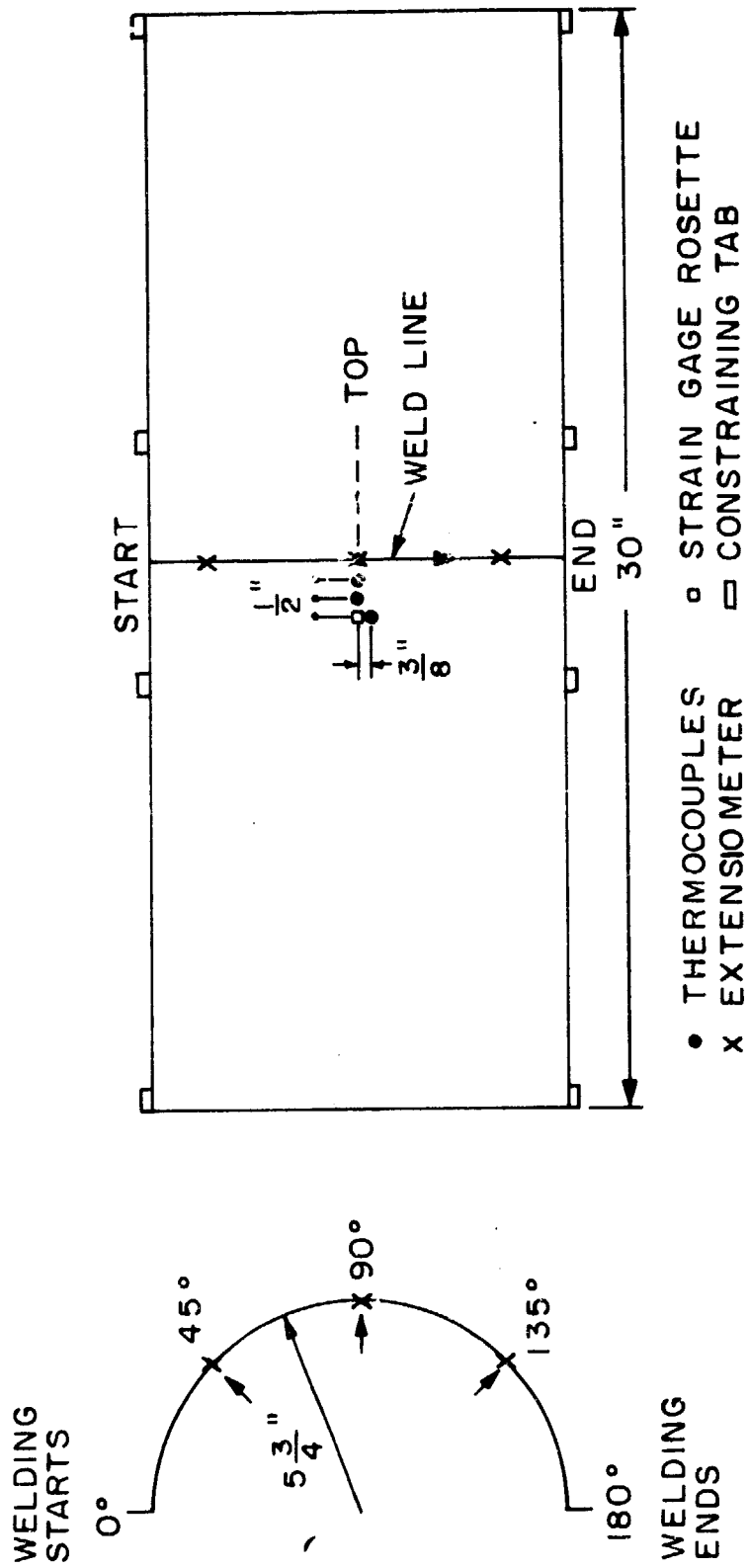


FIGURE 2 SPECIMEN DIMENSIONS AND GAGE LOCATIONS

As shown in Figure 2, four thermocouples were attached to the locations on the weld line and of 0.5, 1.0, and 1.5 inches from the weld line, respectively. The first three were located 9 inches ahead of the starting point of welding along the circumferential weld line. The fourth is on 3/8 inch from the mid-point of the weld line in the welding direction.

Temperature changes were measured by these thermocouples and recorded by the Honeywell No. 1508 visicorder. Figure 3 shows the instrumentation circuit to calibrate the thermocouples.

Strain Measurement: A SR-4 foil 45° rosette was used to measure thermal strain changes during welding. Table 2 provides gage properties. Figure 2 shows the location of the rosette gage attached 9 inches from the starting point of welding in the welding direction and 1.5 inch away of the weld line.

The rosette gage was connected into a Potentiometric Circuit, balanced and calibrated as indicated schematically in Figure 4.

The observed values through the gage consist of mechanical strains and so-called "apparent strains". Figure 5 provided by the gage manufacturer shows a curve of apparent strains vs. temperature obtained by a test gage mounted on a 2024 aluminum alloy sample. Since the 6061 aluminum alloy has a greater coefficient of thermal expansion than the 2024 test sample, a connection to the curve mentioned above has been made.

From reference (18) the following relation was used as the apparent strain for the 6061 aluminum alloy:

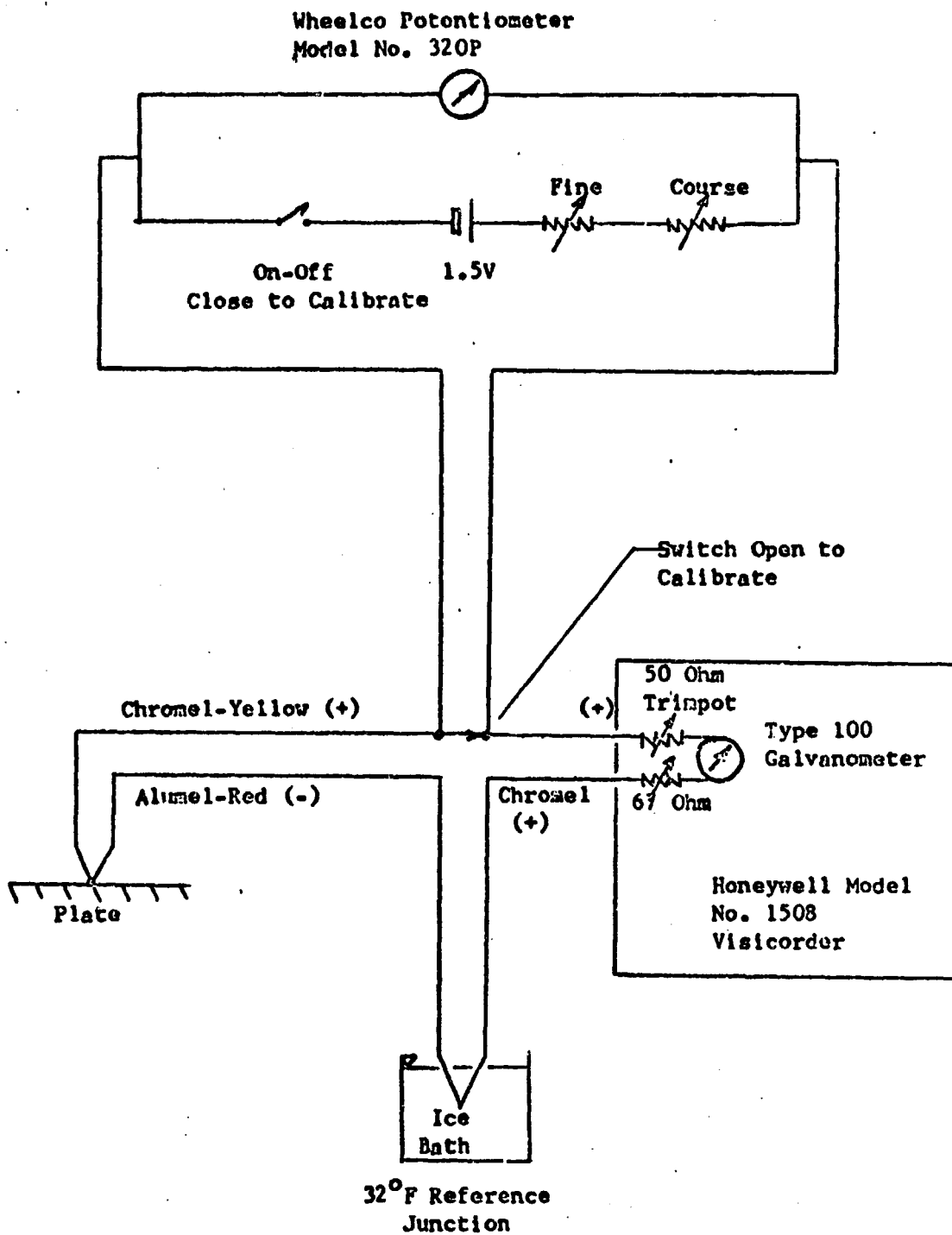


FIGURE 3
Thermocouple Instrumentation Circuit

TABLE 2
Gage Properties

<u>Gage</u>	<u>SR-4 Rosette</u>	<u>SR-4 Gage</u>
Designation	FAER-18RB-12S13-ET	FAE-25-12S13L
Manufacturer	BLH Electronics	BLH Electronics
Grid Length (in.)	3/16	1/4
Grid Width (in.)	0.90	0.13
Overall Length (in.)	0.280	0.35
Overall Width (in.)	0.540	0.13
Temperature Range	-50 to +400°F	-50 to +400°F
Resistance	120.	120.
Gage Factor	2.03	2.07
Cement	EPY-600	EPY-600
Protective Covering	BLH Barrier-C	BLH Barrier-C

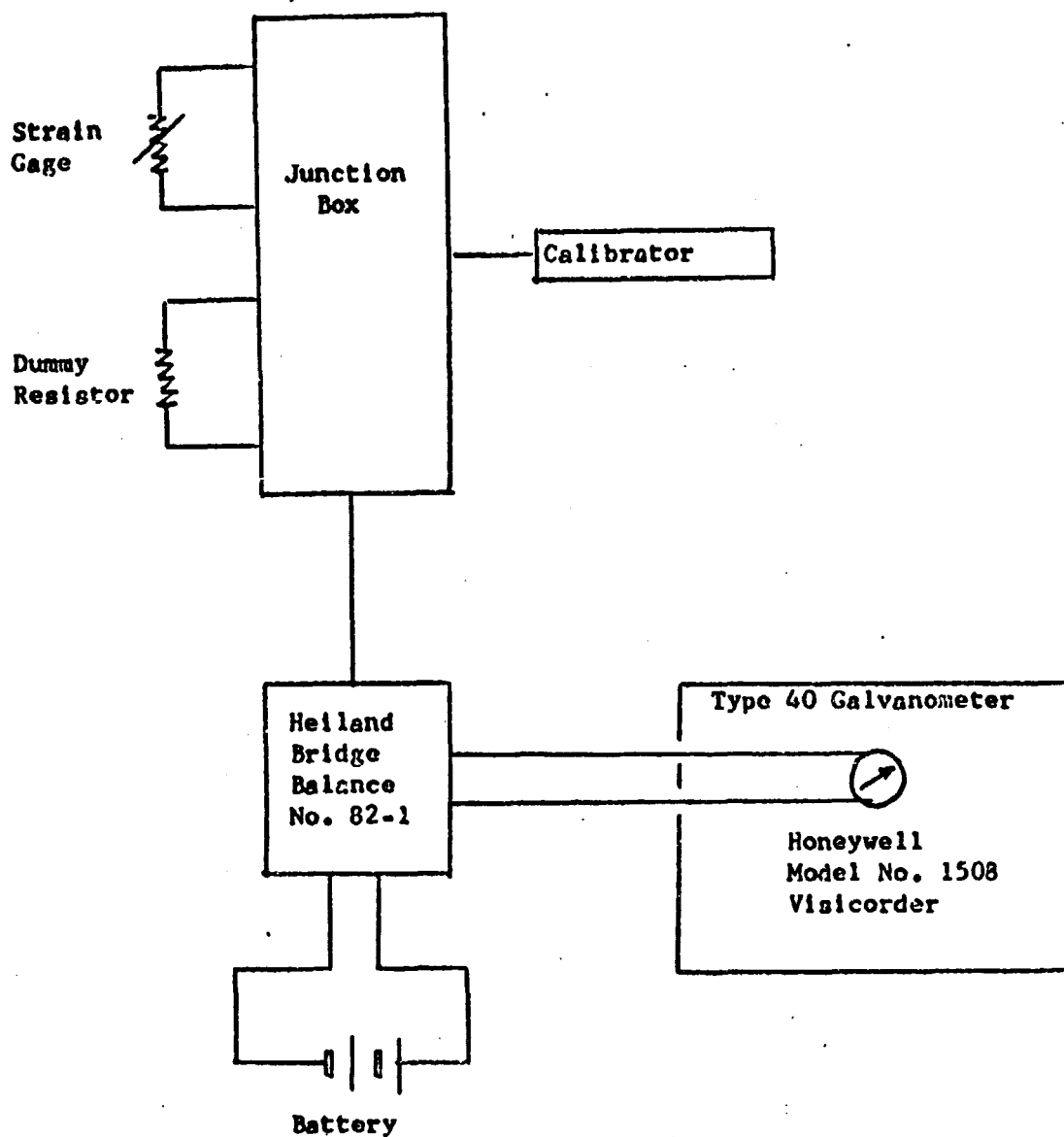
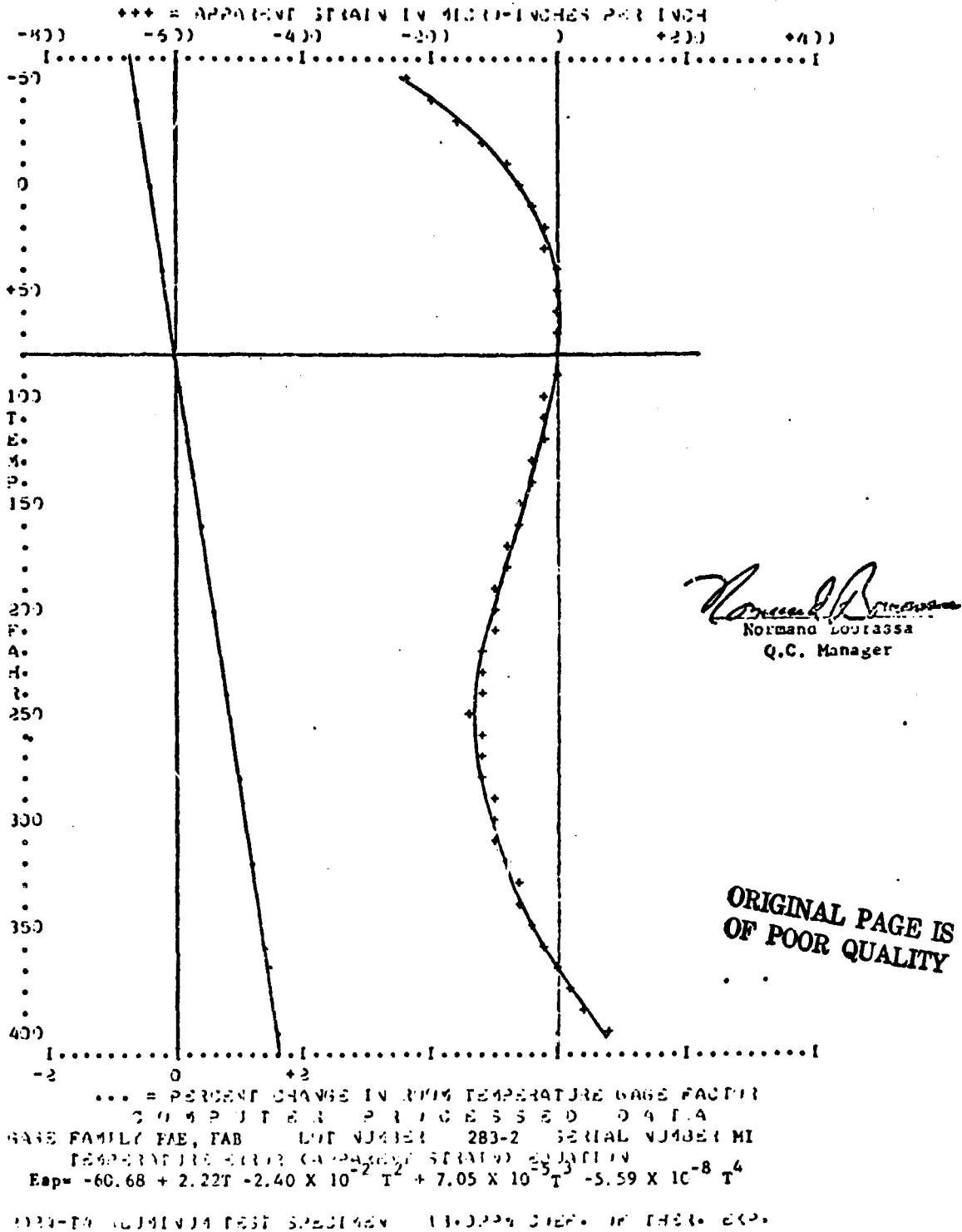


FIGURE 4

Strain Gage Instrumentation Circuit



ORIGINAL PAGE IS
OF POOR QUALITY

FIGURE 5

Apparent strain correction for FAER-18RB-12S13-ET strain gage rosettes utilized in this study.

$$EAP_{6061} - EAP_{2024} + \Delta EAP$$

where

$$EAP_{2024} = -60.68 + 2.22T - 2.40 \times 10^{-2}T^2 \\ + 7.05 \times 10^{-5}T^3 - 5.59 \times 10^{-8}T^4 \\ \Delta EAP = +19.4979 + 0.2463T + 0.9561 \times 10^{-4}T^2 \\ - 0.7879 \times 10^{-7}T^3 + 0.5303 \times 10^{-10}T^4$$

EAP_{6061} , EAP_{2024} , and ΔEAP denote the apparent strains in the 6061 and 2024 aluminum alloys and a connection due to the difference of thermal expansion coefficient between the two materials, respectively.

Temperature change at the gage location is estimated from the observed curve at the thermocouple NO. 4, considering a time lag between temperature curves at the gage and the thermocouple locations.

Subtracting the apparent strain, EAP_{6061} from the actual strain measured, the mechanical strain is provided.

Since the gage is mounted on the upper surface of the specimen, the mechanical strain includes the bending strain as well as the membrane strain.

The strain due to bending is easily discriminated from the strain due to membrane deformation, only if the elastic deformation is assumed to occur in the sample specimen.

Displacement Measurement: Figure 6 shows a sketch of the extensometer used in this experiment. SR-4 foil single element gages were located on both sides of a spring steel ribbon and con-

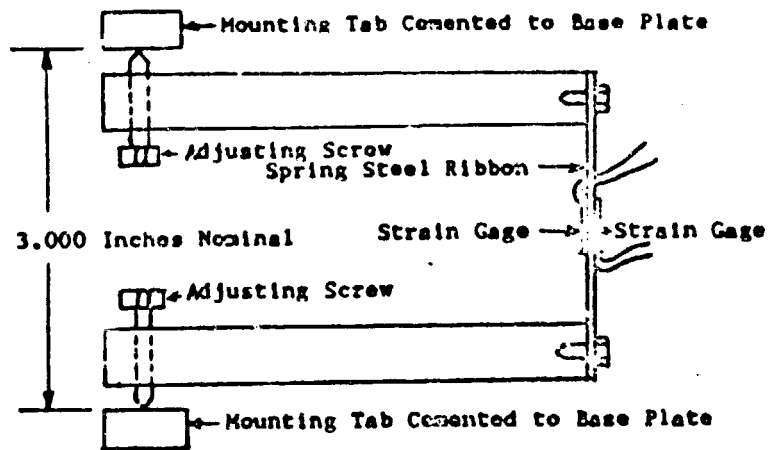


FIGURE 6

Extensometer. The adjusting screws are set so that the spring holds extensometer firmly in place.

ORIGINAL PAGE IS
OF POOR QUALITY

nected into adjacent legs of the resistance circuit shown in Figure 6 of the above paragraph. The net effect of such a set-up is to double the bending sensitivity and null the stretching sensitivity. The gage properties are provided in Table 2.

The extensimeters were set up to measure deformation of the shell specimen along the weld line. Three locations at every 45° angle from the starting point of welding were chosen on the lower surface of the specimen. X1, X2, and X3 in Figure 2 show the extensimeter locations. The extensimeters were mounted between tabs on the specimen and a small shell-shape attachment welded on a base plate.

3.3 Experimental Operation

The experimental operation is shown schematically in Figure 7. The test specimen, clamped to a base steel plate, was put on a brick bed. Arc voltage and amperage were preset at 20 volts and 180 amperes, respectively. Welding of the specimen was manually performed by use of GTA (gas tungsten-arc) welding.

The visicorder was actuated to start recording the changes of temperature, strain and displacement at points of interest. Then the welding torch started moving from one end to another along the circumference at the middle length of the shell. When the welding head reached the end of the shell specimen the arc was extinguished and the specimen allowed to cool. The recorder continued to monitor the gages for twenty minutes until conditions appeared stable.

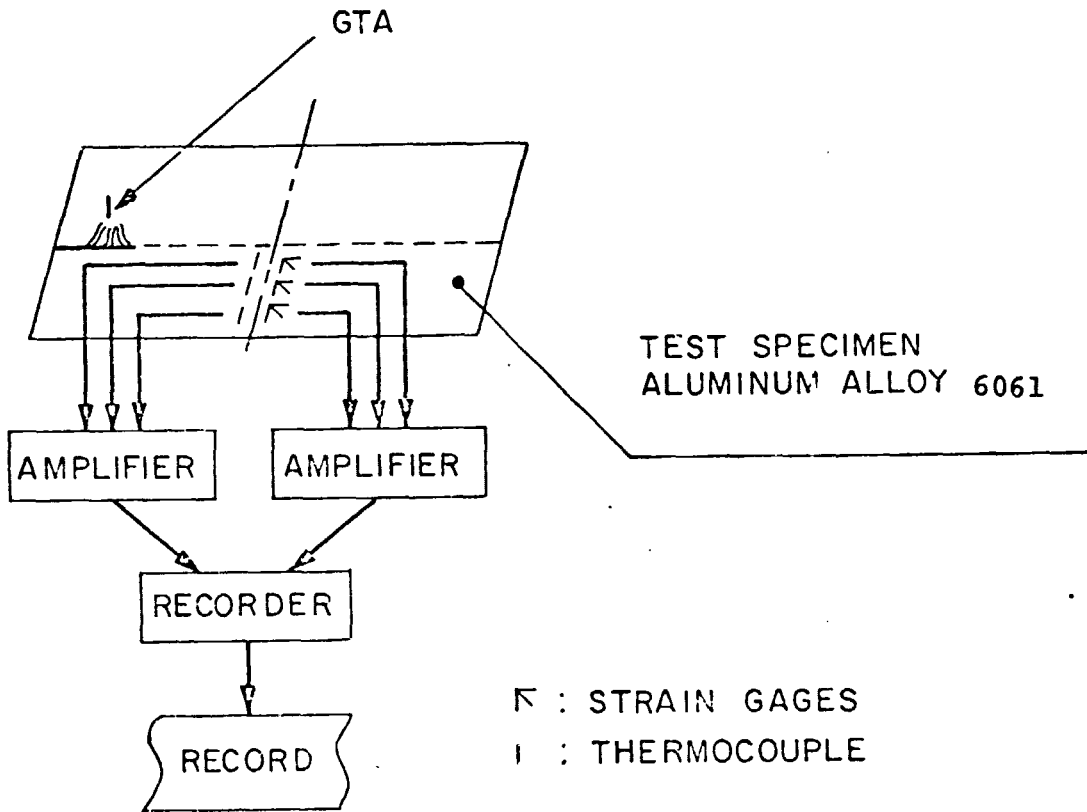


FIGURE 7
Schematic of Apparatus and Procedure

To measure welding speed, time was marked on the recording sheet when the arc passed every forth-five degrees of angle from the starting end. This was done because manually operated welding was difficult to keep a constant welding speed.

3.4 Experimental Results and Analyses

Welding Parameters: Several parameters associated with the experiment are discussed below.

Arc Efficiency: Figure 12 shows the temperature history at thermocouple NO.4 locating 1.5 inch from the weld line. From Figures 8 and 12, the arc efficiency in this GTA welding is estimated of 0.28%.

Welding Speed: Welding was performed manually. In the first three-fourths of the girth length of the shell specimen, welding speed was approximately 0.123 inch/sec and in the last one-fourth, 0.238 inch/sec.

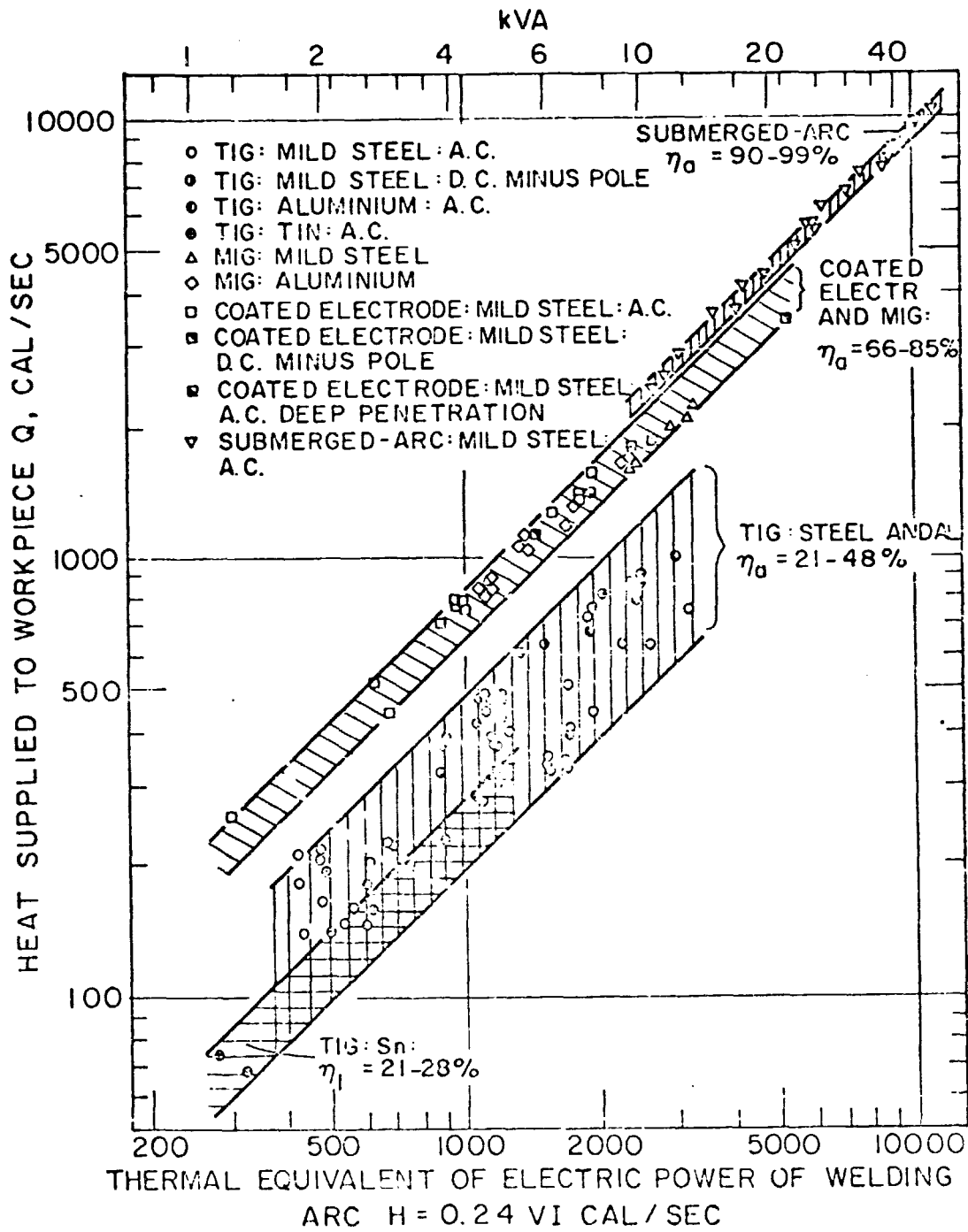
Figures 9 to 17 provide experimental results. The results are described below.

Temperature Histories: Figures 9 to 12 show the temperature histories at the points of 0.0, 0.5, 1.0, and 1.5 inches from the weld line from start of welding to 220 seconds, respectively.

Figure 9 shows temperature measured on the weld line did not reach the melting point. The maximum temperature observed was about 610°F.

The analytical solution^{*} of a moving point heat source on

*The arc efficiency is assumed to be 28% as mentioned before.



**ORIGINAL PAGE IS
OF POOR QUALITY**

FIGURE 8

Measured values of efficiency for various processes and materials (taken from reference 19)

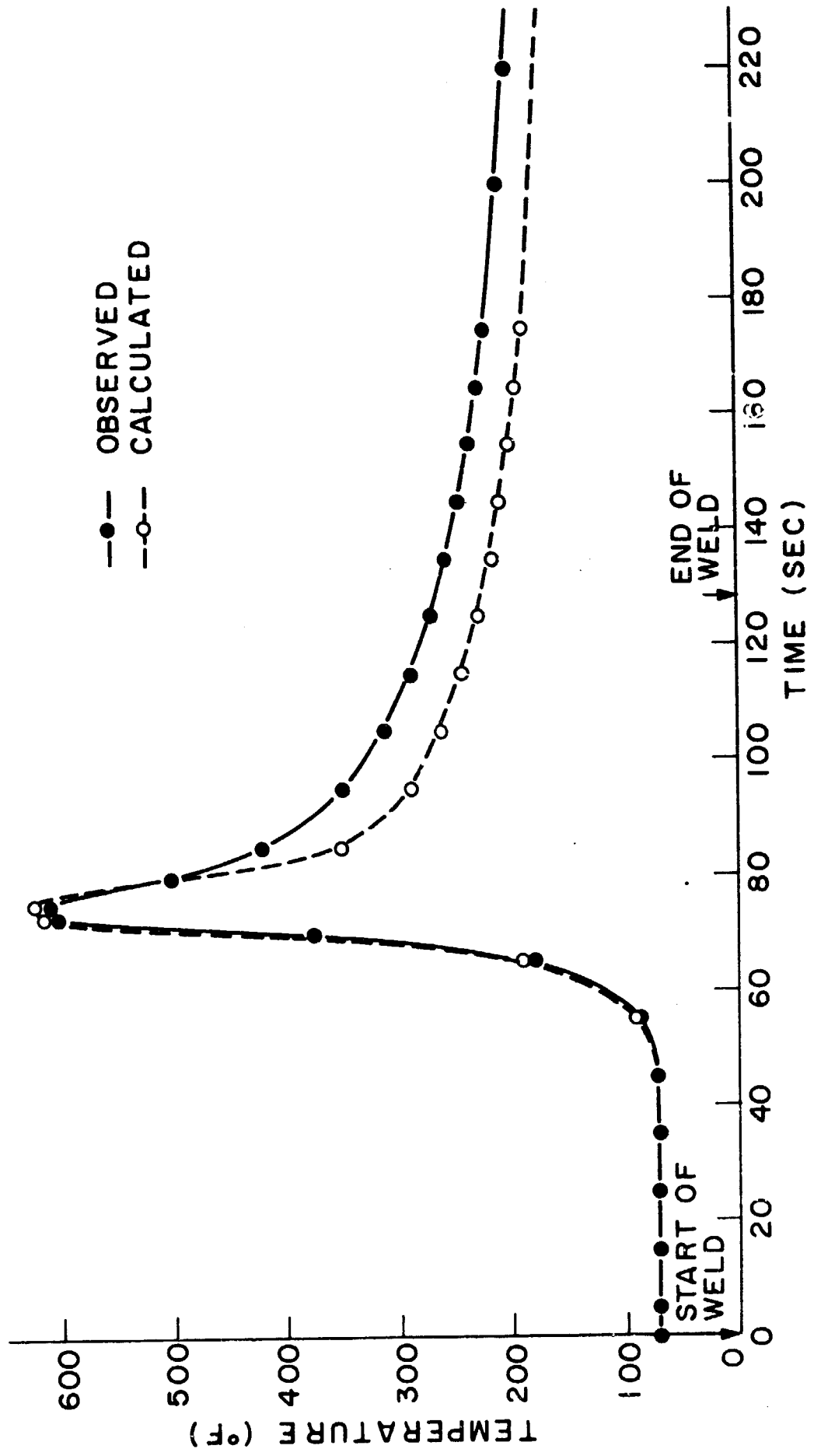


FIGURE 9 TEMPERATURE HISTORY ON WELD LINE

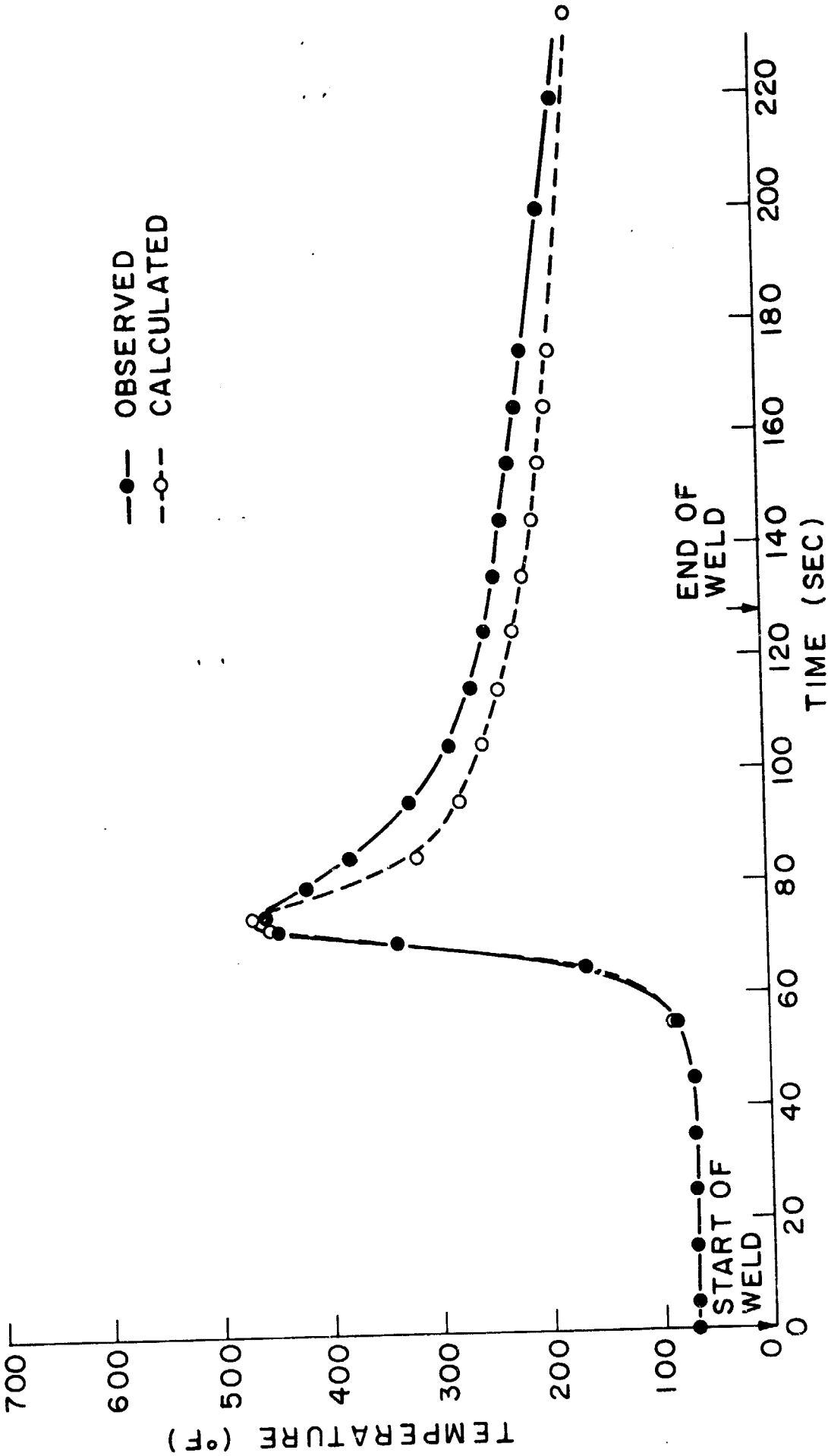


FIGURE 10 TEMPERATURE HISTORY 0.5 INCH FROM WELD LINE

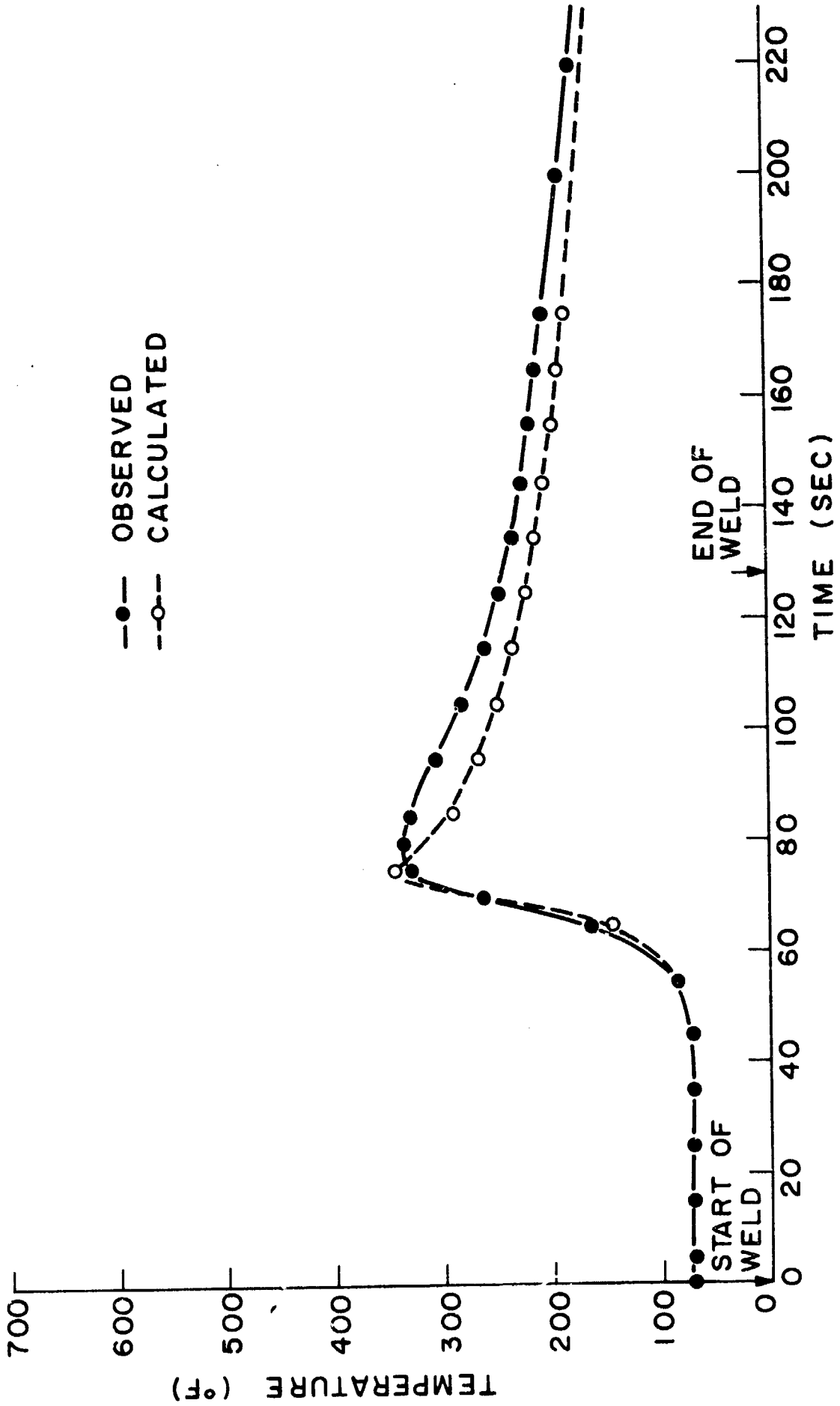


FIGURE 11 TEMPERATURE HISTORY 1.0 INCH FROM WELD LINE

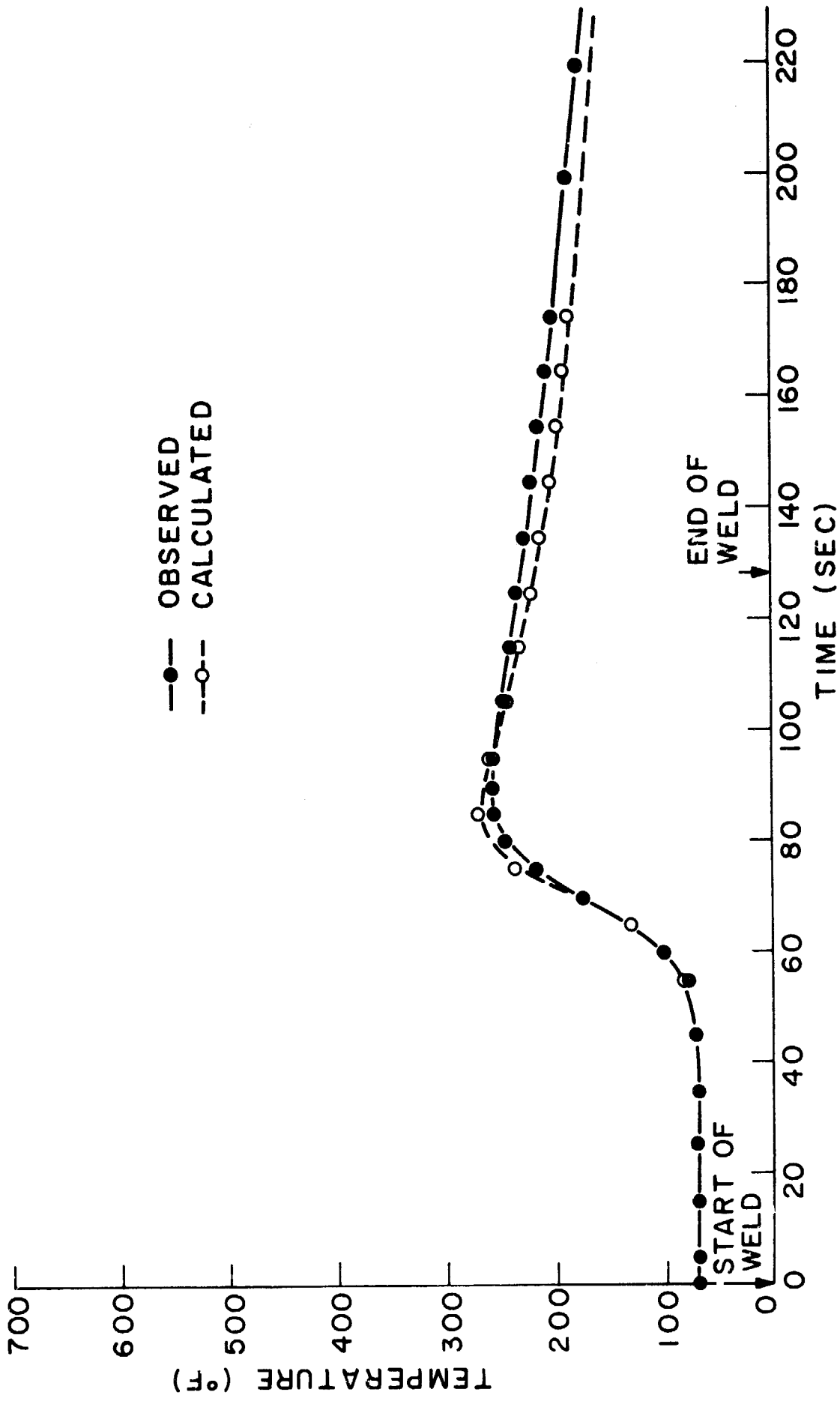


FIGURE 12 TEMPERATURE HISTORY 1.5 INCH FROM WELD LINE

a plate gives good agreement with experimental result at the point of 1.5 inch from the weld line.

Figure 12 shows the comparison between the observed and calculated results. However, poor agreement is obtained on results at the other points. In order to solve this discrepancy, another approach based on a combination of the analytical and the experimental results is made.

The experimental results obtained at the four locations are used to obtain correction factors to the analytical results inside of 1.5 inch from the weld line. The results obtained by this method are shown in Figure 9 to 11.

Strain Changes: A rosette gage is located at a point of 1.5 inch from the weld line and of the middle in girth of the shell specimen, as shown in Figure 2.

Figure 13 to 15 show changes of the circumferencial, the longitudinal, and the shear strains at the point, respectively. These values consist of stretching and bending effects. As seen from the figures, the longitudinal and the shear strain changes have the similar trend to a bead-on-plate results⁽¹⁸⁾. On the other hand, the circumferencial strain shows the more complicated change. This change obviously shows the coupled effects of stretching and bending which is longer in a shell specimen than a plate specimen.

Displacements: The extensimeters were located at three points under the shell shown in Figure 2. The extensimeter results are given in Figure 16. Displacement trend is described as follows:

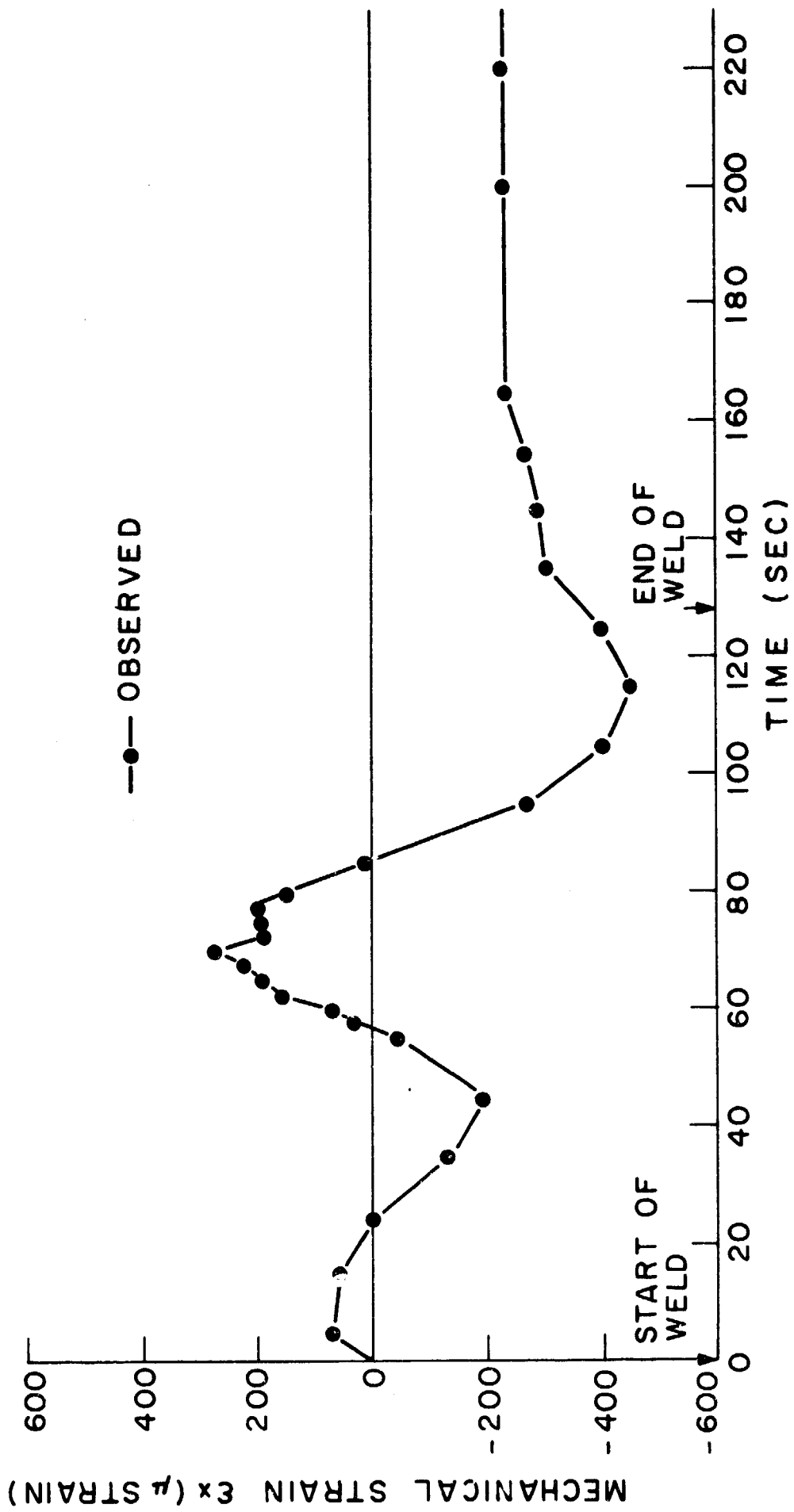


FIGURE 13 CIRCUMFERENTIAL MECHANICAL STRAIN

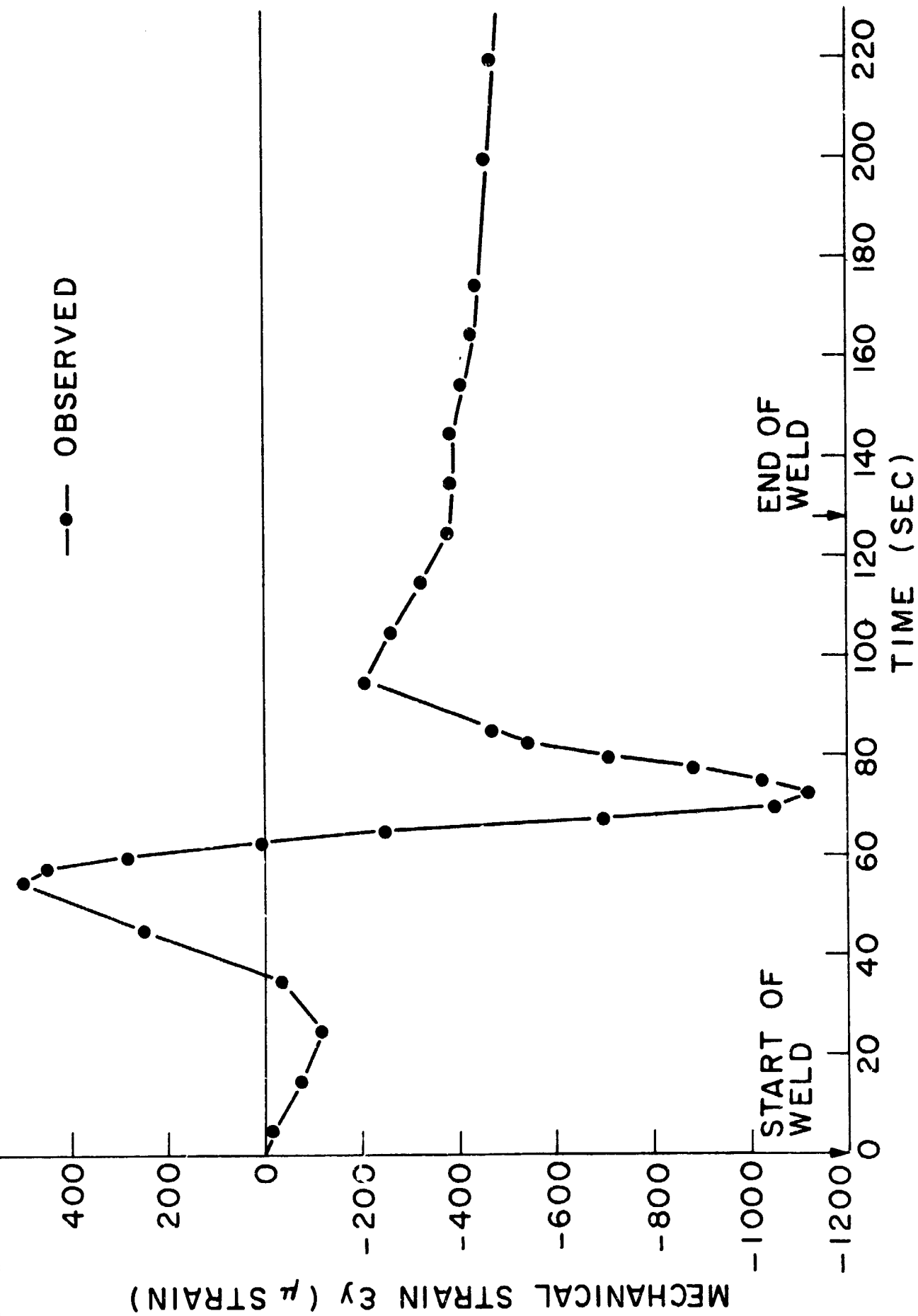


FIGURE 14 LONGITUDINAL MECHANICAL STRAIN

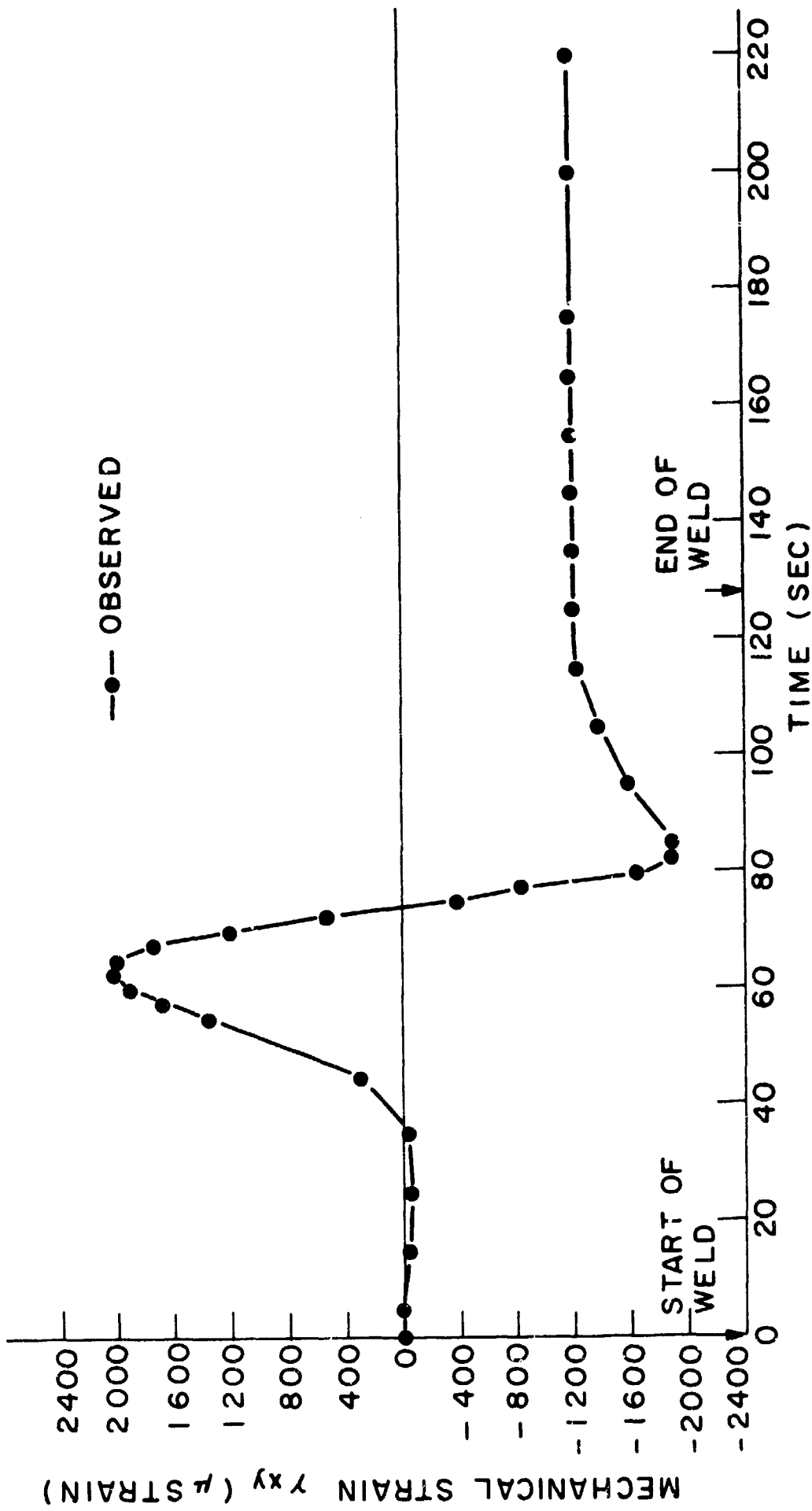


FIGURE 15 MECHANICAL SHEAR STRAIN

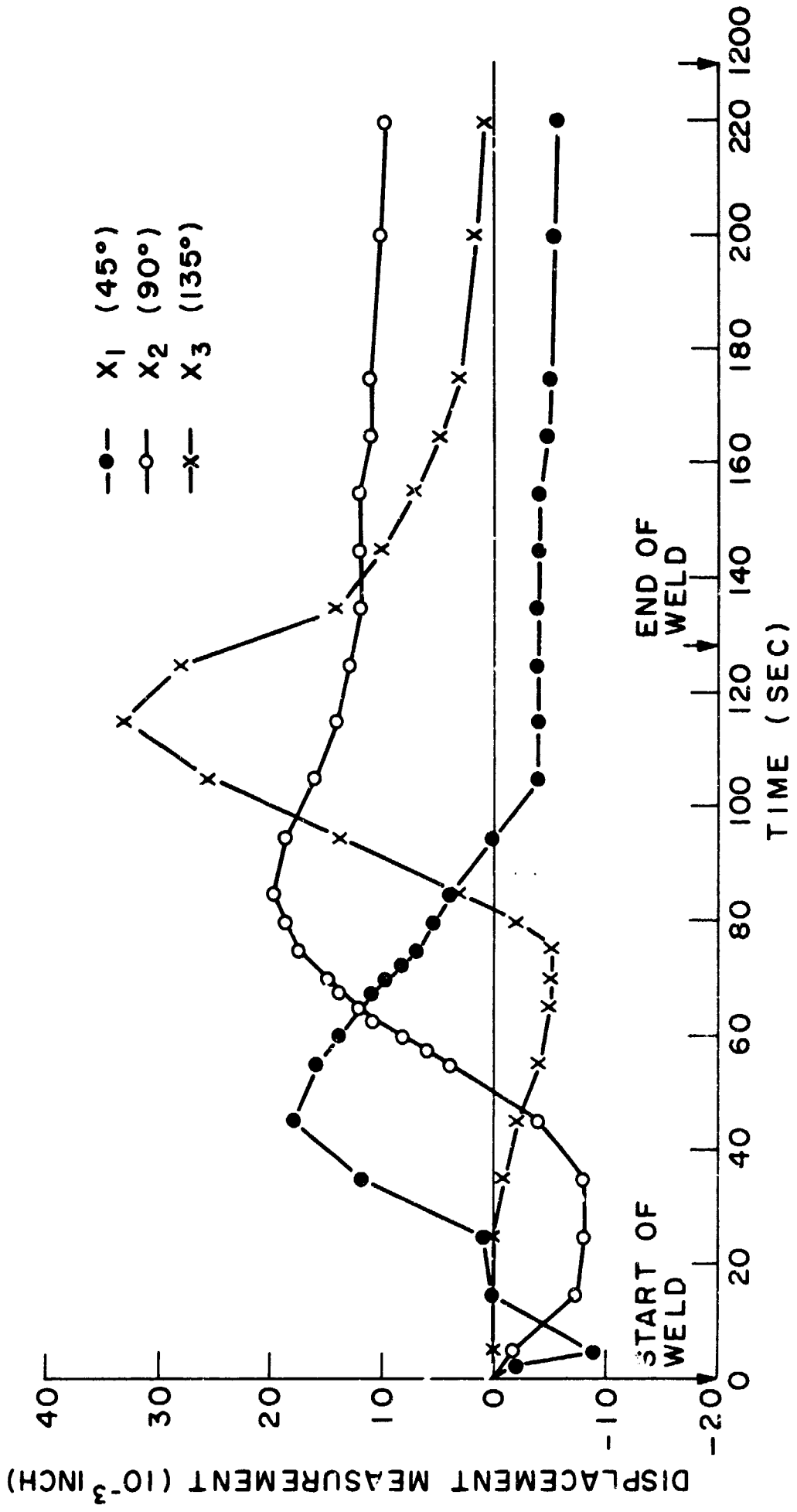


FIGURE 16 EXTENSOMETER MEASUREMENTS
NOTE: POSITIVE VALUE DENOTES UPWARD DISPLACEMENT IN THE
RADIAL DIRECTION OF THE SHELL

When the arc approaches to the extensiometer locations, they displace downward. Then the points turn the displacement direction to upwards. The largest displacement at the points in question is observed in a short time after the arc passes through the points. It is predicted from the figure that the middle point along the weld line almost returns to the original position while both sides of the middle point deform below the original ones. This result is explained by the shrinkage of the weld line.

Closing Comments: Good agreements were obtained between experimental data on temperature and analytical predictions, as shown in Figure 8 through 11. Unfortunately, however, there was more than an order of magnitude difference between experimental and analytical values on thermal strains and displacements. Apparently, computer programs have not been completely debugged.

We plan to continue the effort to debug the computer program, and we will prepare an additional report to cover this subject as soon as possible.

REFERENCES

- (1) Andrews, J.B., Arita, M. and Masubuchi, K., "Analysis of Thermal Stress and Metal Movement during Welding," NASA Contractor Report NASA CR-61351, prepared for the G.C. Marshall Space Flight Center, December, 1970. (For sale by the National Technical Information Service, Springfield, Virginia 22151.)
- (2) Muraki, T. and Masubuchi, K., Phase Report Under Contract No. NAS8-24365 entitled "Analysis of Thermal Stresses and Metal Movement During Welding," to G.C. Marshall Space Flight Center, NASA from Massachusetts Institute of Technology, June 21, 1973.
- (3) Masubuchi, K., "Control of Distortion and Shrinkage in Welding," Welding Research Council Bulletin 149, April, 1970.
- (4) Masubuchi, K., "Residual Stresses and Distortion in Welded Aluminum Structures and Their Effects on Service Performance," Welding Research Council Bulletin 174, July, 1972.
- (5) Hibbit, H.D., and Marcal, P.V., "A Numerical Thermo-Mechanical Model for the Welding and Subsequent Loading of a Fabricated Structure," Dept. of Navy, NSRDC Contract No. N00014-67-A-0191-006, Technical Report No. 2, March, 1972.
- (6) Ueda, Y., and Yamakawa, T., "Analysis of Thermal Elastic-Plastic Stress and Strain during Welding," Document X-616-71, The International Institute of Welding, 1971.
- (7) Satoh, K., Ueda, Y. and Matsui, S., "1972-73 Literature Survey on Welding Stresses and Strains in Japan," Document X-699-73, presented at the 1973 Annual Assembly of Commission X of the International Institute of Welding.
- (8) Nomoto, T., "Finite Element Analysis of Thermal Stresses During Welding," Ph.D. Thesis, University of Tokyo, 1971.
- (9) Masubuchi, K., Simmons, F.B. and Monroe, R.E., "Analysis of Thermal Stresses and Metal Movement during Welding," Final Report under contract DA-01-021-AMC-14693(Z) from Battelle Memorial Institute to Redstone Scientific Information Center, RSIC-820, July, 1968.
- (10) Masubuchi, K., and Iwaki, T., "Thermo-elastico-plastic Analysis of Orthotropic Plates by the Finite Element Method," Journal of the Society of Naval Architects of Japan, Vol. 130, 195-204, 1971.

- (11) Muraki, T. and Masubuchi, K., "Finite-Element Analysis Based upon the Generalized Variational Principle of Plastic and Elastic Distortion of Plates and Shells," a paper presented at the International Conference on Computer Applications in the Automation of Shipyard Operation and Ship Design, August 28-30, 1973, Tokyo, Japan.
- (12) Masubuchi, K., Andeews, J. B., and Urushihara, A., "Finite Element Analysis of Thermo-elastoplastic Deformations in Butt Welding," Document X-692-73 presented at the 1973 Annual Assembly of Commission X of the International Institute of Welding.
- (13) Masubuchi, K., "Heat Flow in Weldments," a chapter of a text-book under preparation.
- (14) Myers, P. S., Uyehara, O. A., and Borman, G. L., "Fundamentals of Heat Flow in Welding," Welding Research Council Bulletin 123, July, 1967.
- (15) Rosenthal, D., "Mathematical Theory of Heat Distribution During Welding and Cutting," Welding Journal 20(5), Supplement 220s to 234s, 1941.
- (16) Muraki, T. and Masubuchi, K., "Thermal Analysis of M551 Experiment for Materials Processing in Space," Final Report under Contract NAS8-28732 for the G. C. Marshall Space Flight Center, NASA from M.I.T., December, 1973.
- (17) Muraki, T., and Masubuchi, K., "Numerical Analysis of Heat Conduction in Solids - With Special Applications to Welding" under Contract NAS8-28732 for the G. C. Marshall Space Flight Center, NASA from M.I.T., March, 1974.
- (18) Bryan, Jon J., "Analysis of Two Dimensional Strains and Metal Movement During Welding," M.S. Thesis, M.I.T., May, 1973.
- (19) Christensen, N., Davis, V. de L., and Gjermunden, K., "Distribution of Temperatures in Arc Welding," Brih's Welding Journal, 12(2), 54-75 (1965).